MOLECULAR AND CELLULAR BIOLOGY, Dec. 2011, p. 4692–4705 Vol. 31, No. 23
0270-7306/11/$12.00 doi:10.1128/MCB.05979-11

Osteoclast Progenitors Reside in the Peroxisome Proliferator-Activated Receptor γ-Expressing Bone Marrow Cell Population▽

Wei Wei,[1] Daniel Zeve,[2] Xueqian Wang,[1] Yang Du,[1] Wei Tang,[2] Paul C. Dechow,[5] Jonathan M. Graff,[2,3,4] and Yihong Wan[1]*

Department of Pharmacology,[1] Department of Developmental Biology,[2] Department of Molecular Biology,[3] and Department of Internal Medicine,[4] University of Texas Southwestern Medical Center, Dallas, Texas 75390, and Department of Biomedical Sciences, Baylor College of Dentistry, Texas A&M University Health Sciences Center, Dallas, Texas 75246[5]

Received 21 July 2011/Returned for modification 20 August 2011/Accepted 18 September 2011

Osteoclasts are bone-resorbing cells essential for skeletal development, homeostasis, and regeneration. They derive from hematopoietic progenitors in the monocyte/macrophage lineage and differentiate in response to RANKL. However, the precise nature of osteoclast progenitors is a longstanding and important question. Using inducible peroxisome proliferator-activated receptor γ (PPARγ)-tTA TRE-GFP (green fluorescent protein) reporter mice, we show that osteoclast progenitors reside specifically in the PPARγ-expressing hematopoietic bone marrow population and identify the quiescent PPARγ$^+$ cells as osteoclast progenitors. Importantly, two PPARγ-tTA TRE-Cre-controlled genetic models provide compelling functional evidence. First, Notch activation in PPARγ$^+$ cells causes high bone mass due to impaired osteoclast precursor proliferation. Second, selective ablation of PPARγ$^+$ cells by diphtheria toxin also causes high bone mass due to decreased osteoclast numbers. Furthermore, PPARγ$^+$ cells respond to both pathological and pharmacological resorption-enhancing stimuli. Mechanistically, PPARγ promotes osteoclast progenitors by activating GATA2 transcription. These findings not only identify the long-sought-after osteoclast progenitors but also establish unprecedented tools for their visualization, isolation, characterization, and genetic manipulation.

Bone is a dynamic tissue that constantly remodels itself by balancing osteoclast-mediated bone resorption and osteoblast-mediated bone formation. Osteoclasts derive from hematopoietic progenitors (5) in the monocyte/macrophage lineage (41, 47); in contrast, osteoblasts are of mesenchymal lineage (38). Physiological osteoclast functions are essential for skeletal development, homeostasis, and regeneration in response to injury. However, pathological increases in osteoclast activities are associated with several diseases, including osteoporosis, arthritis, and bone metastasis of cancers (35).

Osteoclast lineage specification is a multistep process that requires osteoclast progenitor commitment (41, 47), macrophage colony-stimulating factor (M-CSF)-mediated osteoclast precursor proliferation (57), and RANKL (receptor activator of NF-κB ligand)-mediated osteoclast differentiation (8, 29, 56). Although the discovery of RANKL has revolutionized research in osteoclast biology, RANKL mainly acts at later stages of osteoclastogenesis. The cellular identity and the precise nature of the *bona fide* osteoclast progenitors are underexplored. Previous studies have elegantly characterized the cell surface markers that enrich osteoclast progenitors using flow cytometry (25); however, tools are lacking to label osteoclast progenitors *in vivo* for visualization, isolation, and lineage tracing, as well as to genetically manipulate osteoclast progenitors for functional characterization.

Peroxisome proliferator-activated receptor γ (PPARγ) is a member of the nuclear receptor family of transcription factors that can be activated by lipophilic ligands, including the diabetic drug rosiglitazone (BRL, or Avandia) (18, 49). Previous studies showed that PPARγ is highly expressed in both monocyte/macrophage precursors and mature osteoclasts (39, 48, 52). Loss of PPARγ function in mouse hematopoietic lineages causes osteoclast defects manifested as osteopetrosis (52). Gain of PPARγ function by pharmacological activation enhances osteoclastogenesis and bone resorption in mice and humans (52, 53, 59). These findings provide important mechanistic understanding of the clinically reported bone loss and higher fracture rates in diabetic patients treated with rosiglitazone. Here, we hypothesize that osteoclast progenitors reside in the PPARγ-expressing hematopoietic bone marrow population and that PPARγ regulation goes beyond osteoclast differentiation by also defining the osteoclast progenitors.

MATERIALS AND METHODS

Mice. PPARγ-tTA TRE-H2BGFP mice (46), flox-DTA mice (30), and NICD-flox mice (55) have been described previously. PPARγ-tTA TRE-cre mice were bred with flox-DTA mice to generate PTDTA mice. PPARγ-tTA TRE-cre mice were bred with NICD-flox mice to generate PTNICD mice. All experiments were performed using littermate cohorts. All protocols for mouse experiments were approved by the Institutional Animal Care and Use Committee of the University of Texas Southwestern Medical Center.

Bone analyses. To evaluate bone volume and architecture by micro-computed tomography (μCT), mouse tibiae were fixed in 70% ethanol and scanned using a Scanco μCT-35 instrument (Scanco Medical) at several resolutions for both overall tibial assessment (14-μm resolution) and structural analysis of trabecular and cortical bone (7-μm resolution). Trabecular bone parameters were calculated using the Scanco software to analyze the bone scans from the trabecular region directly distal to the proximal tibial growth plate. Histomorphometric analyses were conducted using Bioquant Image Analysis software (Bioquant). TRAP (tartrate-resistant acid phosphatase) staining of osteoclasts was performed using a leukocyte acid phosphatase staining kit (Sigma). ALP staining of

* Corresponding author. Mailing address: Department of Pharmacology, UT Southwestern Medical Center, 6001 Forest Park Road, Room ND8.502B, Dallas, TX 75390-9041. Phone: (214) 645-6062. Fax: (214) 645-6067. E-mail: yihong.wan@utsouthwestern.edu.

▽ Published ahead of print on 26 September 2011.

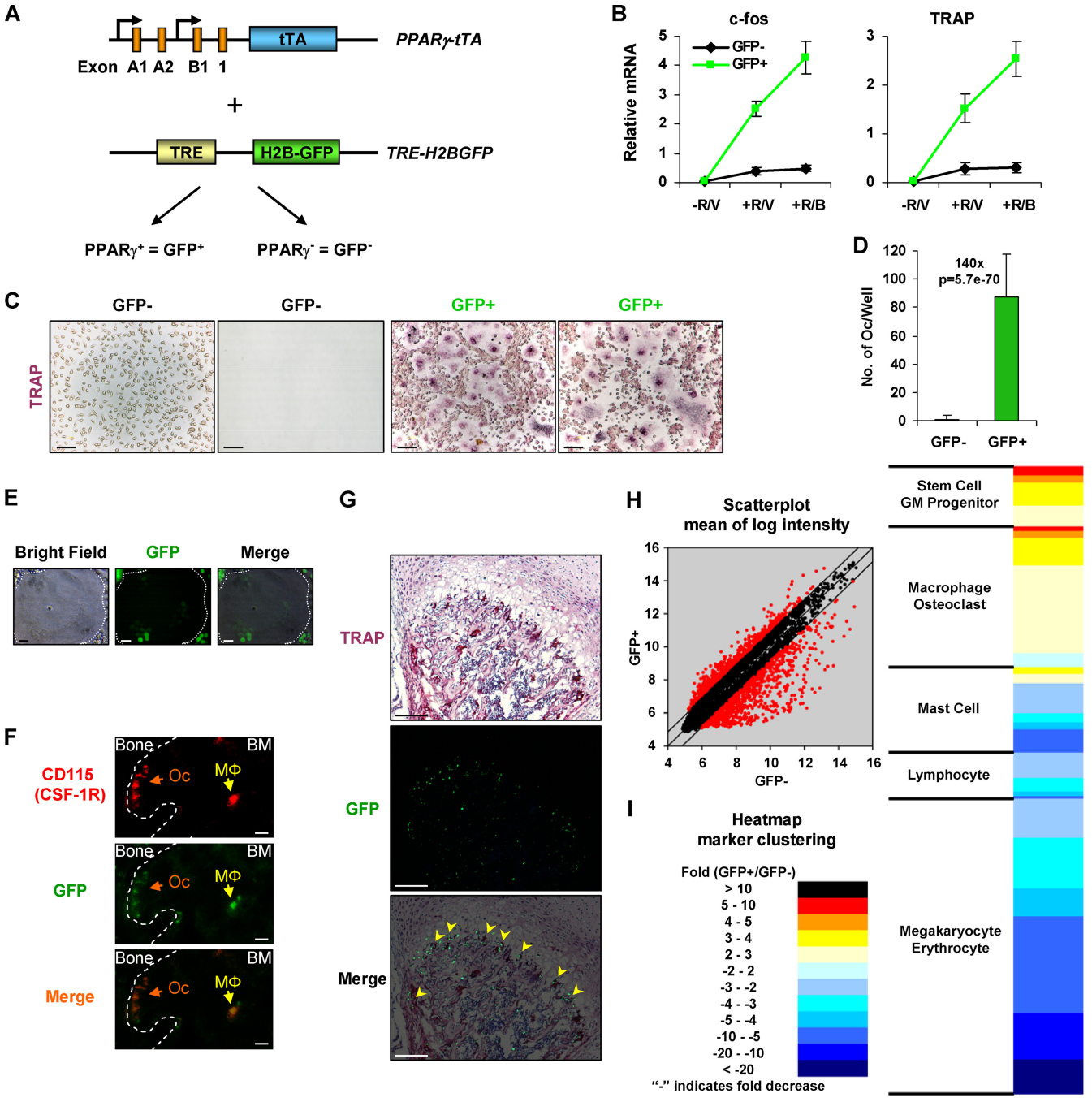

FIG. 1. The osteoclast lineage resides in the PPARγ-expressing bone marrow population. (A) Schematic diagram of the PPARγ-tTA TRE-H2BGFP reporter mouse model. (B) Osteoclast marker expression in *ex vivo* bone marrow differentiation cultures ($n = 3$). V, vehicle; R, RANKL; B, BRL (rosiglitazone). The error bars indicate SD. (C and D) Osteoclast colony formation assay. Bone marrow cells were purified with a 40-μm cell strainer, FACS sorted into GFP^+ and GFP^- populations, and seeded at 100 cells/well. (C) Representative images of the TRAP-stained differentiation cultures. Scale bars, 25 μm. Two wells each for GFP^- cells (left) and GFP^+ cells (right) are shown; the second image from the left shows a GFP^- well with no macrophage colony formation. (D) Average number of mature osteoclasts (Oc) per well ($n = 96$), showing that the frequency of osteoclast formation was 140-fold higher in the GFP^+ population than in the GFP^- population ($P = 5.7e{-}70$). (E to G) The osteoclast lineage resides in the PPARγ-expressing bone marrow population *in situ*. (E) Multinucleated mature osteoclasts (outlined by dashed lines) differentiated from unsorted bone marrow of PPARγ-GFP mice *ex vivo* were GFP^+. Scale bars, 25 μm. (F) $CD115^+$ monocyte/macrophage precursors (MΦ) in the bone marrow (BM) and $CD115^+$ multinucleated osteoclasts at the bone/marrow boundary were GFP^+. Scale bars, 4 μm. (G) The $TRAP^+$ (purple) osteoclasts colocalized with the GFP^+ cells *in vivo* (indicated by yellow arrowheads). Scale bars, 25 μm. (H and I) Microarray analysis of $PPAR\gamma^+$ (GFP^+) and $PPAR\gamma^-$ (GFP^-) hematopoietic bone marrow cells ($n = 2$, from 2 independent reporter mice). (H) Scatterplot of the genes up- or downregulated in the GFP^+ population (≥1.8-fold; $P \leq 0.05$) (red). (I) Heat map illustrating the expression changes of cell-type-specific marker genes.

osteoblasts was performed using an alkaline phosphatase staining kit (Sigma). As a bone resorption marker, urinary C-terminal telopeptide fragments of the type I collagen (CTX-1) was measured with the RatLaps enzyme immunoassay (EIA) kit (Immunodiagnostic Systems) and normalized by urinary creatinine measured with the Infinity Creatinine Reagent (Thermo Scientific). As a bone formation marker, serum osteocalcin was measured with the mouse osteocalcin EIA kit (Biomedical Technologies Inc.).

***Ex vivo* osteoclast differentiation.** Osteoclasts were differentiated from mouse bone marrow cells as described previously (52, 53). Briefly, bone marrow cells were purified with a 40-μm cell strainer to remove mesenchymal cells, differentiated with 40 ng/ml of M-CSF (R&D Systems) in α minimal essential medium (α-MEM) containing 10% fetal bovine serum (FBS) for 3 days and then with 40 ng/ml of M-CSF and 100 ng/ml of RANKL (R&D Systems) for 3 days (unless otherwise stated), with or without BRL (1 μM) throughout the time course. Mature osteoclasts were identified as multinucleated (>3 nuclei) $TRAP^+$ cells. Osteoclast differentiation was quantified by the RNA expression of RANKL-induced transcription factors and osteoclast function genes using reverse transcription-quantitative PCR (RT-QPCR) analysis.

Osteoclast precursor proliferation assay. Osteoclast precursor proliferation was quantified using a bromodeoxyuridine (BrdU) cell proliferation assay kit (GE Healthcare Life Sciences) (6). Mouse bone marrow cells were treated with M-CSF (40 ng/ml) for 3 days to stimulate osteoclast precursor expansion. On day 4, the cells were M-CSF starved for 6 h to synchronize the cell cycle. The cells were then restimulated with M-CSF for 4 h to induce S phase, during which BrdU was provided in the culture medium and integrated into the DNA of the proliferating cells. Osteoclast precursor proliferation was quantified as BrdU incorporation using the BrdU enzyme-linked immunosorbent assay (ELISA) in the kit.

Gene expression analyses. RNA was reverse transcribed into cDNA using an ABI High Capacity cDNA RT Kit and analyzed using real-time quantitative PCR (SYBR green) in triplicate. All RNA expression was normalized by ribosomal protein L19.

Promoter analyses. Promoter sequence alignment was performed using Vector NTI Advanced 11 AlignX software (Invitrogen). Chromatin immunoprecipitation (ChIP) assays were performed using fluorescence-activated cell sorter (FACS)-sorted green fluorescent protein-positive (GFP^+) and GFP^- mouse bone marrow cells as previously described (52). The antibodies used were PPARγ, PU.1 (Santa Cruz), acetyl-histone H3 (Upstate/Millipore), and IgG negative control (BD Biosciences). ChIP output was quantified by real-time PCR in triplicate and normalized by 10% input.

Transfection. Bone marrow cells were purified with a 40-μm cell strainer to remove mesenchymal cells, sorted by FACS into GFP^+ and GFP^- populations, and cultured with 40 ng/ml M-CSF overnight. Cells in suspension were removed, and adherent cells were transfected in the presence of 40 ng/ml M-CSF, using FuGene HD (Roche) for 3 days before RANKL-induced osteoclast differentiation. The transfection efficiency was >50%. For GATA2 gain of function, a plasmid encoding full-length GATA2 (Open Biosystems) or vector control was transfected. For GATA2 loss of function, small interfering RNA (siRNA) for GATA2 (siGATA2) or control siRNA (siCtrl) (Santa Cruz) was transfected.

Flow cytometry. The FACS analyses of bone marrow cells were performed using a BD FACScan flow cytometer and phycoerythrin (PE)-conjugated antibodies (all from BD Pharmingen). The FACS sorting of GFP^+ and GFP^- bone marrow cell populations was performed using a MoFlo Cell Sorter (Beckman Coulter).

Statistical analyses. All statistical analyses were performed with Student's *t* test, and the results are represented as means and standard deviations (SD).

RESULTS

Identification of osteoclast progenitors by *in vivo* labeling. To test this hypothesis, we employed our PPARγ-GFP reporter mice (PPARγ-tTA TRE-H2BGFP) (46). In these mice, a tet transactivator cassette (tTA) was inserted into the endogenous PPARγ locus. When combined with the tTA-responsive H2BGFP transgenic allele (TRE-H2BGFP) (26, 51), the bigenic mice marked PPARγ-expressing cells with GFP (Fig. 1A). We isolated GFP^+ cells from the hematopoietic bone marrow population by FACS (http://www4.utsouthwestern.edu/wanlab/publications.htm) and compared their osteoclastogenic potential with that of GFP^- cells using an *ex vivo* osteoclast differentiation assay. Expression of the osteoclast markers c-fos and TRAP (Fig. 1B), as well as Ctsk, Calcr, and CAR2 (not shown), indicated that GFP^+ cells differentiated into osteoclasts, while such activity appeared to be lacking in GFP^- cells.

To quantify osteoclast colony formation, we sorted GFP^+ and GFP^- bone marrow cells, plated them at 100 cells/well in 96-well plates, and cultured them with M-CSF until 50% confluence before RANKL stimulation. After 11 days, we stained the cells for TRAP and quantified mature osteoclasts ($TRAP^+$ and >3 nuclei) in each well. The majority of the GFP^+ cells in each well had already formed osteoclasts, and the remaining mononuclear cells were $TRAP^+$ preosteoclasts in the process of maturation (Fig. 1C). For GFP^+ wells, both macrophage and osteoclast colonies developed at 100% (96/96); in contrast, 55% (53/96) of GFP^- wells developed $TRAP^-$ macrophage colonies, and only 7% (4/96) formed osteoclasts. The number of osteoclasts per well was also significantly higher for GFP^+ than for GFP^- wells; as a result, the frequency of osteoclast formation was 140-fold higher for GFP^+ cells (Fig. 1D), indicating that >99% of osteoclast progenitors/precursors were $PPAR\gamma^+$. These results show that the osteoclast lineage resides in the GFP^+ bone marrow population *ex vivo*.

Imaging analyses further supported the notion that the osteoclast lineage was derived from GFP^+ cells *ex vivo* and *in vivo*. First, we performed *ex vivo* osteoclast differentiation using the unsorted bone marrow cells of PPARγ-GFP mice. The multinucleated osteoclasts developed in culture were all GFP^+ (Fig. 1E). Second, we performed immunostaining of the femoral sections for CD115 (M-CSF receptor [M-CSFR]), a marker for the monocyte/macrophage lineage. The $CD115^+$ multinucleated osteoclasts at the bone/marrow junction were GFP^+, and notably, the $CD115^+$ monocyte/macrophage precursors in the bone marrow also expressed GFP (Fig. 1F). Third, we performed TRAP staining as an independent method to identify osteoclasts. The $TRAP^+$ osteoclasts also colocalized with GFP^+ cells (Fig. 1G). We also observed GFP^+ bone marrow cells that were $TRAP^-$, which represent putative osteoclast progenitors and precursors (Fig. 1G). Thus, the osteoclast lineage resides in the GFP^+ bone marrow population *in situ*.

To compare the gene expression profiles of GFP^+ and GFP^- cells, we performed microarray analysis. Approximately 800 genes were up- or downregulated in the GFP^+ population by ≥1.8-fold ($P \leq 0.05$) (Fig. 1H). The GFP^+ cells displayed increased expression of stem cell/granulocyte-monocyte (GM) progenitor (26 genes) and macrophage/osteoclast (61 genes) markers and decreased expression of lymphocyte (20 genes), mast cell (37 genes), and megakaryocyte/erythrocyte (128 genes) markers (Fig. 1I) (http://www4.utsouthwestern.edu/wanlab/publications.htm). This suggests that (i) the $PPAR\gamma^+$ population is enriched for stem/progenitor cells and (ii) PPARγ expression specifically directs hematopoiesis toward the monocyte/macrophage lineage but away from lymphoid or other myeloid lineages, including megakaryocytes, erythrocytes, and mast cells. Consistently, methylcellulose colony-forming assays showed that GFP^+ cells generated more macrophage colonies but fewer granulocyte, erythrocyte, and lymphocyte colonies than GFP^- cells (http://www4.utsouthwestern.edu/wanlab/publications.htm). Together, these data

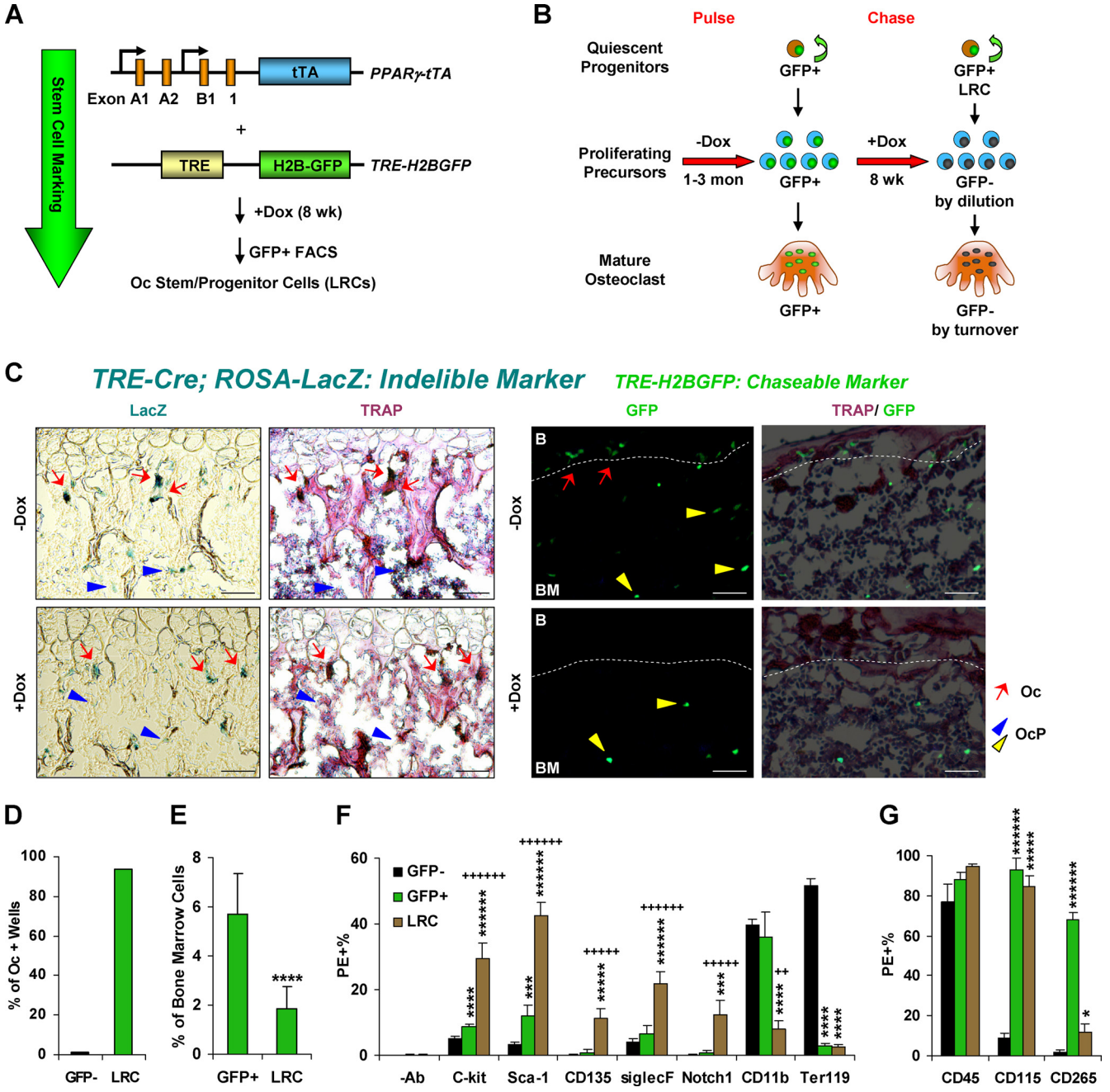

FIG. 2. Osteoclast progenitors reside in quiescent PPARγ$^+$ bone marrow cells. (A) Schematic diagram of the *in vivo* marking of osteoclast stem/progenitor cells. (B) A pulse-chase strategy labels the quiescent PPARγ$^+$ stem/progenitor cells as LRCs. (C) Lineage tracing of mature osteoclasts from PPARγ$^+$ progenitors using an indelible LacZ reporter (left) and a chaseable GFP reporter (right). OcP, osteoclast progenitor/precursors; B, bone; BM, bone marrow. Scale bars, 25 μm. (D) Percentage of LRCs or GFP$^-$ cells that formed osteoclasts when plated at a single cell per well ($n = 96$). (E to G) Flow cytometry analyses of the LRC, GFP$^+$, and GFP$^-$ bone marrow populations ($n = 6$). The error bars indicate SD. (E) Percentages of total GFP$^+$ cells and LRCs in the bone marrow. (F) Percentage of cells expressing stem/progenitor cell markers (C-Kit, Sca-1, CD135, SiglecF, or Notch1), macrophage marker (CD11b), or erythrocyte marker (Ter119) in each population. For *P* values, the asterisks compare total GFP$^+$ cells or LRCs with GFP$^-$ cells and the pluses compare LRCs with total GFP$^+$ cells. (G) Percentage of cells expressing CD45, CD115 (M-CSFR; c-fms), or CD265 (RANK). ⋆, $P < 0.05$; ++, $P < 0.01$; ⋆⋆⋆, $P < 0.005$; ⋆⋆⋆⋆, $P < 0.001$; ⋆⋆⋆⋆⋆ or +++++, $P < 0.0005$; ⋆⋆⋆⋆⋆⋆ or ++++++, $P < 0.0001$.

indicate that we have identified the osteoclast progenitors in the PPARγ-expressing hematopoietic bone marrow cell population, and we can prospectively visualize, isolate, and characterize the osteoclast progenitors using the PPARγ-GFP reporter mice.

Osteoclast progenitors reside in quiescent PPARγ$^+$ bone marrow cells. The inducible PPARγ-tTA TRE-H2BGFP reporter mice afforded a tool for osteoclast stem/progenitor cell marking by H2BGFP label retention, a quality that is often indicative of quiescent stem/progenitor cell popula-

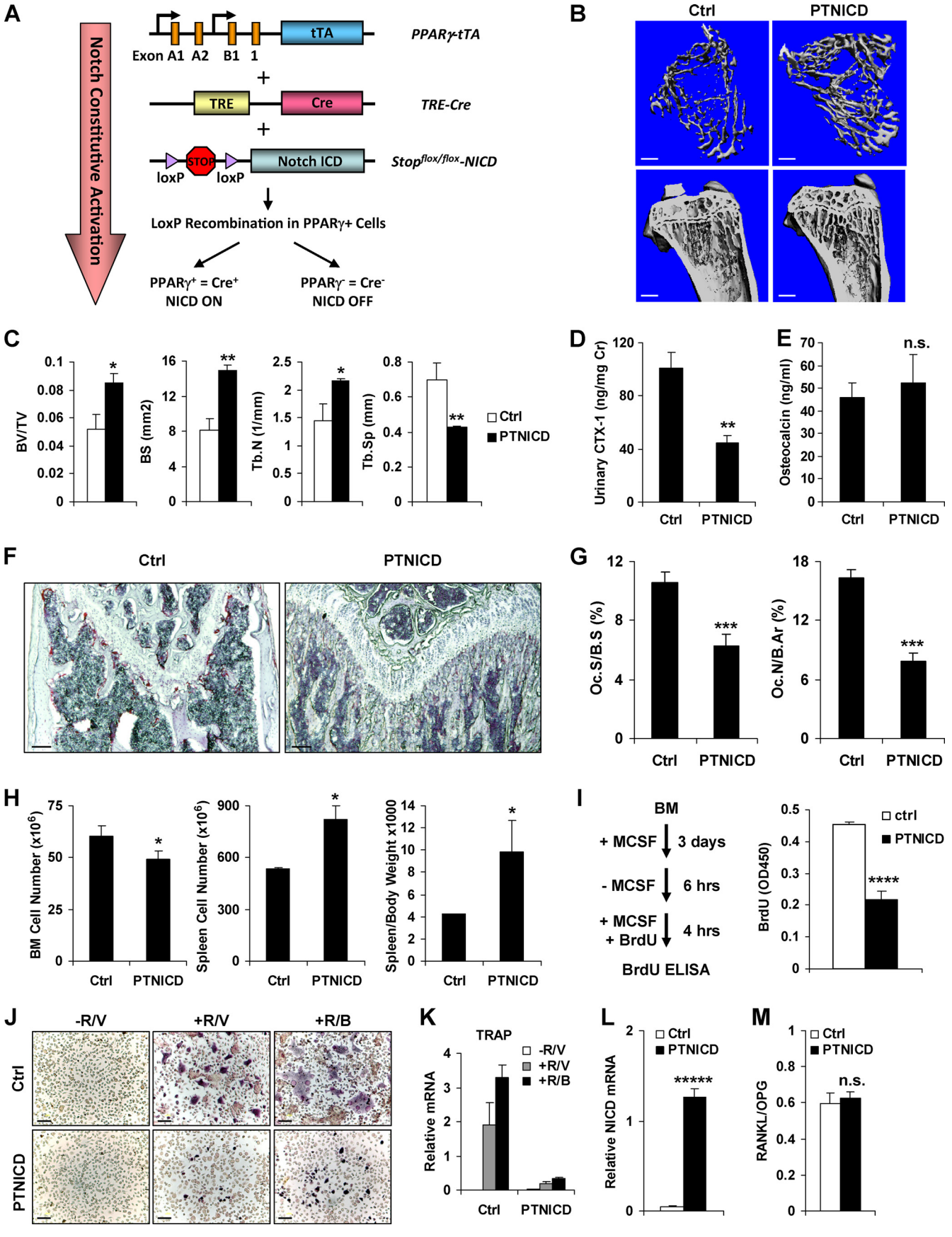

tions (51). Histone H2B-GFP has been well characterized as a stable protein and a sensitive marker for chromosome dynamics in living cells (26, 51). In the absence of doxycycline (Dox), all PPARγ$^+$ cells are labeled with GFP. When tTA activity is suppressed by Dox, only postmitotic and quiescent stem/progenitor cells retain the label, as H2BGFP is diluted in proliferating cells (26; http://www4.utsouthwestern.edu/wanlab/publications.htm) (Fig. 2A). Thus, we employed a pulse-chase strategy to distinguish slow-cycling (quiescent progenitor) from fast-cycling (proliferating precursor) cells (Fig. 2B). We first pulsed the reporter mice by allowing GFP expression in all PPARγ$^+$ cells (−Dox) and then chased with Dox for 8 weeks to block new H2BGFP expression and thus mark only the label-retaining cells (LRCs). Terminally differentiated osteoclasts are also GFP$^+$ and no longer proliferate. However, osteoclasts undergo constant turnover, with a half-life of 1.3 days in mice (32). Thus, the initial GFP$^+$ osteoclasts were eliminated by apoptosis and replaced by osteoclasts differentiated from GFP$^-$ precursors by the end of the 8-week Dox chase (Fig. 2B). Previous studies have shown that 4 weeks to 4 months of Dox chase is sufficient to label progenitors as LRCs (26). In our study, we consistently Dox chased the mice for 8 weeks to ensure both proliferating precursors and mature osteoclasts became GFP$^-$. Therefore, this pulse-chase strategy labels osteoclast progenitors as LRCs in the bone marrow.

To determine whether mature osteoclasts can be lineage traced to PPARγ$^+$ progenitors, we employed both a proliferation-sensitive chaseable marker (H2BGFP) and a proliferation-insensitive indelible marker (LacZ) for PPARγ$^+$ cells (http://www4.utsouthwestern.edu/wanlab/publications.htm). In the PPARγ-tTA TRE-H2BGFP reporter, only quiescent PPARγ$^+$ progenitors remain GFP$^+$ after Dox suppression of tTA activity, whereas in the PPARγ-tTA TRE-Cre ROSA-LacZ reporter, all cells that originate from PPARγ$^+$ progenitors before Dox suppression at postnatal day 2 (P2) remain LacZ$^+$, since the cre-flox recombination event is irreversible (http://www4.utsouthwestern.edu/wanlab/publications.htm). Thus, the combination of these two markers allows lineage tracing of PPARγ$^+$ progenitors. The results showed that mature osteoclasts indeed originated from PPARγ$^+$ progenitors, because they became GFP$^-$ but still remained LacZ$^+$ after the Dox chase (Fig. 2C). To quantify the purity of osteoclast progenitors in the hematopoietic LRC population, we FACS sorted LRCs and plated them at a single cell per well in 96-well plates to assess their ability to differentiate into osteoclasts. The results showed that 94% of LRCs (+Dox) formed osteoclasts (90/96) whereas only 1% of GFP$^-$ cells (−Dox) formed osteoclasts (1/96) (Fig. 2D), indicating that the LRCs specifically labeled osteoclast progenitors.

We next further characterized the LRC (+Dox), GFP$^+$ (−Dox), and GFP$^-$ (−Dox) populations by FACS analysis. First, LRCs represented ~1/3 of the total GFP$^+$ cells (Fig. 2E). Second, stem/progenitor cell markers, including c-Kit (2, 24, 60), Sca-1 (44), CD135 (33), Siglec-F (3), and Notch-1 (6), were further enriched in the LRCs compared with either total GFP$^+$ or GFP$^-$ (Fig. 2F) cells, whereas the macrophage marker CD11b was reduced in LRCs (Fig. 2F), indicating an increase in non-lineage-committed progenitors (4). Third, the erythrocyte marker Ter119 was excluded from both total GFP$^+$ cells and LRCs (Fig. 2F). Fourth, >95% of LRCs expressed the leukocyte common antigen CD45, a marker found on all cells of hematopoietic origin except mature erythrocytes and platelets (23) but not on cells of mesenchymal origin (9), demonstrating that the LRCs purified by our method did not contain significant mesenchymal cell types (Fig. 2G). Fifth, 93% of total GFP$^+$ cells and 85% of LRCs expressed CD115 (M-CSFR; c-fms), and 68% of total GFP$^+$ cells and 12% of LRCs expressed CD265 (RANK), a receptor required for osteoclast precursors but not for myeloid progenitors or macrophages (15) (Fig. 2G). These results not only confirmed the microarray analysis (Fig. 1I) showing that the GFP$^+$ population was highly enriched for the stem/progenitor cells of the monocyte/macrophage lineage, but also identified the LRC subpopulation as the osteoclast progenitors.

Constitutive activation of Notch signaling in PPARγ$^+$ cells causes high bone mass. Notch signaling is a key regulator of osteoblastogenesis (17); however, the cell-autonomous function of Notch in osteoclastogenesis is incompletely understood. We found that Notch1 expression was 15-fold higher in LRCs than in total GFP$^+$ cells (Fig. 2F), indicating that Notch signaling may regulate the quiescence-to-proliferation switch of the osteoclast progenitors. A previous study showed that loss of Notch function by Notch1 to -3 deletion enhances osteoclastogenesis by promoting osteoclast precursor proliferation (6). Nonetheless, the effect of gain of Notch function in the osteoclast lineage is unknown. Thus, if PPARγ$^+$ cells are *bona fide* osteoclast progenitors, then Notch activation in these cells should impair osteoclastogenesis by restraining the quiescence-to-proliferation switch. To test this hypothesis, we ex-

FIG. 3. Notch activation in PPARγ-expressing cells causes high bone mass. (A) Schematic diagram of PTNICD mice. (B and C) μCT analysis of the tibiae from PTNICD or control mice (5 months old; male; $n = 6$). (B) Representative images of the trabecular bone of the tibial metaphysis (top; scale bar, 10 μm) and the entire proximal tibia (bottom; scale bar, 1 mm). Ctrl, control. (C) Quantification of trabecular bone volume and architecture. BS, bone surface; Tb.N, trabecular number; Tb.Sp, trabecular separation. The error bars indicate SD. (D) Urinary CTX-1 (normalized to urinary creatinine) ($n = 6$). (E) Serum osteocalcin ($n = 6$). (F and G) Bone histomorphometry ($n = 6$). (F) Representative images of TRAP-stained femoral sections. Scale bar, 100 μm. (G) Quantification of osteoclast surface (Oc.S/B.S) and number (Oc.N/B.Ar); B.Ar, bone area. (H) PTNICD mice exhibited extramedullary hematopoiesis in the spleen ($n = 6$). (I) Osteoclast precursor proliferation was decreased in the PTNICD cultures. (Left) Schematic diagram of the proliferation assay. (Right) Quantification of BrdU incorporation ($n = 3$). (J and K) Osteoclast differentiation was blunted in the PTNICD culture. (J) Representative images of TRAP-stained osteoclast differentiation cultures. Scale bar, 25 μm. (K) Representative osteoclast marker expression ($n = 3$). R, RANKL; V, vehicle; B, BRL. (L) NICD expression in control or PTNICD differentiation culture ($n = 3$). (M) Tibial RANKL/OPG mRNA ratio in control or PTNICD mice ($n = 3$). *, $P < 0.05$; **, $P < 0.01$; ***, $P < 0.005$; ****, $P < 0.001$; *****, $P < 0.0005$; n.s., nonsignificant ($P > 0.05$).

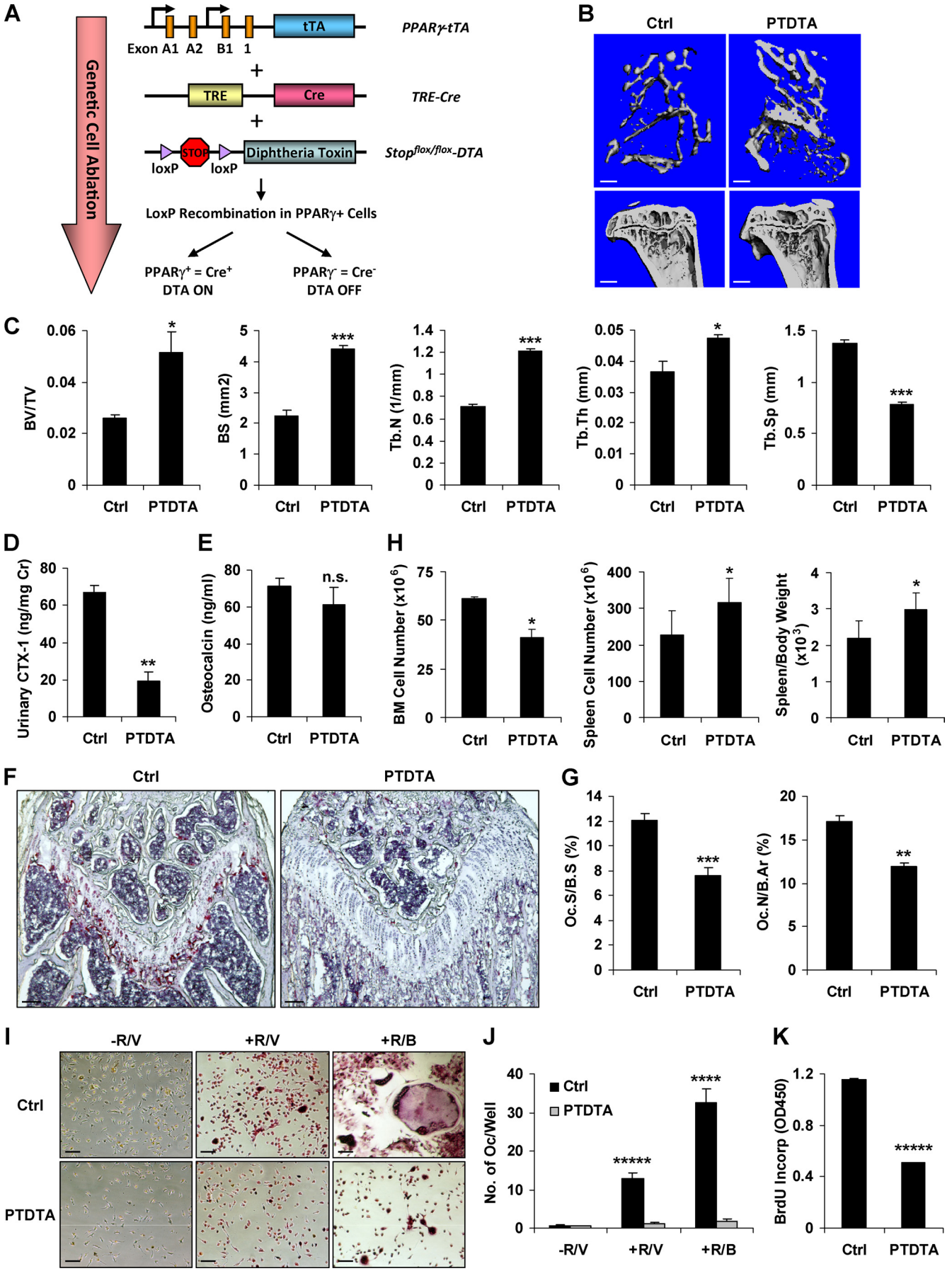

ploited the PPARγ-tTA system, which enables not only osteoclast progenitor marking but also genetic manipulation therein. Specifically, PPARγ-tTA TRE-Cre mice permit rapid translation to *in vivo* models harboring flox-mediated inducible gene deletion or activation in osteoclast progenitors. To express a constitutively active Notch intracellular domain (NICD) in the osteoclast lineage, we bred PPARγ-tTA TRE-Cre mice with $Stop^{flox/flox}$-NICD mice (55) to generate PTNICD mice (Fig. 3A).

Skeletal examinations indicated that the PTNICD mice developed high bone mass due to osteoclast defects. First, μCT imaging revealed a significant increase in trabecular bone in the PTNICD mice (Fig. 3B and C). Second, ELISA analyses showed that the bone resorption marker CTX-1 was markedly decreased by 56% (Fig. 3D) while the bone formation marker osteocalcin was unaltered (Fig. 3E). Third, histomorphometry showed that osteoclast surface and number (Oc.S/B.S and Oc.N/B.Ar) were significantly reduced (Fig. 3F and G), while osteoblast surface and number (Ob.S/B.S and Ob.N/B.Ar) were unaltered (http://www4.utsouthwestern.edu/wanlab/publications.htm). As often observed in osteopetrotic mice, PTNICD mice also exhibited extramedullary hematopoiesis in the spleen (Fig. 3H). These data suggested that the increased bone mass resulted mainly from decreased osteoclast numbers and bone resorption.

To assess the stage at which Notch activation blocks osteoclastogenesis and the cell-autonomous nature of the effects, we analyzed the osteoclast progenitors *ex vivo*. M-CSF-mediated osteoclast precursor proliferation was markedly reduced in the PTNICD cultures (Fig. 3I). Consistently, the bone marrow cells from PTNICD mice exhibited lower expression of RANK, PPARγ1, and c-fms than controls (http://www4.utsouthwestern.edu/wanlab/publications.htm). Moreover, RANKL-mediated and BRL-stimulated osteoclast differentiation was also blunted (Fig. 3J), and induction of osteoclast marker genes was severely decreased (Fig. 3K). NICD expression was significantly increased (Fig. 3L). In contrast, the tibial RANKL/OPG mRNA ratio was unaltered (Fig. 3M). These results all indicate that the impaired bone resorption in PTNICD mice was due to an osteoclast-autonomous defect. The simultaneous reduction in precursor proliferation and osteoclast differentiation suggested that Notch activation in $PPAR\gamma^+$ cells prevented the quiescence-to-proliferation switch of the osteoclast progenitors. This was consistent with the previous loss-of-function study showing that Notch is required to maintain the osteoclast stem cell fate (6). Importantly, these results demonstrated that osteoclast progenitors indeed reside in the $PPAR\gamma^+$ bone marrow population *in vivo* and can be marked and genetically manipulated by the PPARγ-tTA system.

Ablation of $PPAR\gamma^+$ cells causes high bone mass. To assess whether selective partial ablation of $PPAR\gamma^+$ cells by "diphtheria toxin attenuated" (DTA) (30) prevents osteoclastogenesis *in vivo*, we bred PPARγ-tTA TRE-Cre mice with $Stop^{flox/flox}$-DTA mice to generate PTDTA mice (Fig. 4A). We found that the PTDTA mice also exhibited high bone mass. μCT revealed higher trabecular bone mass (Fig. 4B and C). CTX-1 was 72% lower (Fig. 4D), while osteocalcin was unaltered (Fig. 4E). Osteoclast surface and numbers were decreased (Fig. 4F and G), while osteoblast surface and numbers were unaltered (http://www4.utsouthwestern.edu/wanlab/publications.htm). Consistently, the PTDTA mice also exhibited extramedullary hematopoiesis in the spleen (Fig. 4H). These data indicated that the increased bone mass in the PTDTA mice was mainly caused by decreased osteoclast numbers and bone resorption.

Because this bone phenotype may be contributed by other PPARγ-expressing cell types, such as adipocytes, we next investigated the cell-autonomous nature of the resorption defects by examining the osteoclastogenic potential of the bone marrow from PTDTA mice *ex vivo*. While many osteoclasts developed in control cultures, few formed in PTDTA cultures (Fig. 4I and J). This was due to cell ablation and, consequently, decreased BrdU incorporation (Fig. 4K). Thus, ablation of $PPAR\gamma^+$ cells severely blunted osteoclastogenesis and bone resorption. Together, the PTNICD and PTDTA genetic models provide compelling *in vivo* evidence that the osteoclast lineage resides in the $PPAR\gamma^+$ bone marrow population under physiological conditions.

Ovariectomy activation of osteoclast progenitors. Estrogen deficiency, from menopause or ovariectomy (OVX), is an important cause of osteoporosis and debilitating fractures. Current notions indicate that estrogen deficiency enhances osteoclast survival (27, 34), but its specific effects on osteoclast progenitors remain unknown. To track the response of the osteoclast lineage to estrogen loss, we performed sham operations or ovariectomies on PPARγ-GFP reporter mice in the setting of placebo or Dox-induced reporter suppression, coupled with BrdU labeling 24 h before FACS analysis (Fig. 5A). We found that OVX significantly increased the GFP^+ bone marrow population by 3.8-fold (Fig. 5B). This increase appeared secondary to enhanced cell proliferation, as both the percentage of $BrdU^+$ cells in the GFP^+ population and the percentage of $BrdU^+/GFP^+$ cells in the entire bone marrow population were elevated by 1.8- and 6.4-fold, respectively (Fig. 5C and D).

Next, we examined the effects of OVX on osteoclast pro-

FIG. 4. Ablation of PPARγ-expressing cells causes high bone mass. (A) Schematic diagram of the PTDTA mice. (B and C) μCT analysis of tibiae from PTDTA or control mice (7 months old; female; $n = 5$). (B) Representative images of the trabecular bone of the tibial metaphysis (top; scale bar, 10 μm) and the entire proximal tibia (bottom; scale bar, 1 mm). (C) Quantification of trabecular bone volume and architecture. The error bars indicate SD. (D) Urinary CTX-1 ($n = 5$). (E) Serum osteocalcin ($n = 5$). (F and G) Bone histomorphometry ($n = 5$). (F) Representative images of TRAP-stained femoral sections. Scale bar, 100 μm. (G) Quantification of osteoclast surface and numbers. (H) PTDTA mice exhibited extramedullary hematopoiesis in the spleen ($n = 5$). (I and J) Osteoclast differentiation was blunted in the PTDTA culture. (I) Representative images of TRAP-stained osteoclast differentiation culture. Scale bar, 25 μm. (J) Numbers of mature osteoclasts per well ($n = 3$). (K) Osteoclast precursor proliferation was decreased in the PTDTA culture ($n = 3$). *, $P < 0.05$; **, $P < 0.01$; ***, $P < 0.005$; ****, $P < 0.001$; *****, $P < 0.0005$; n.s., nonsignificant ($P > 0.05$).

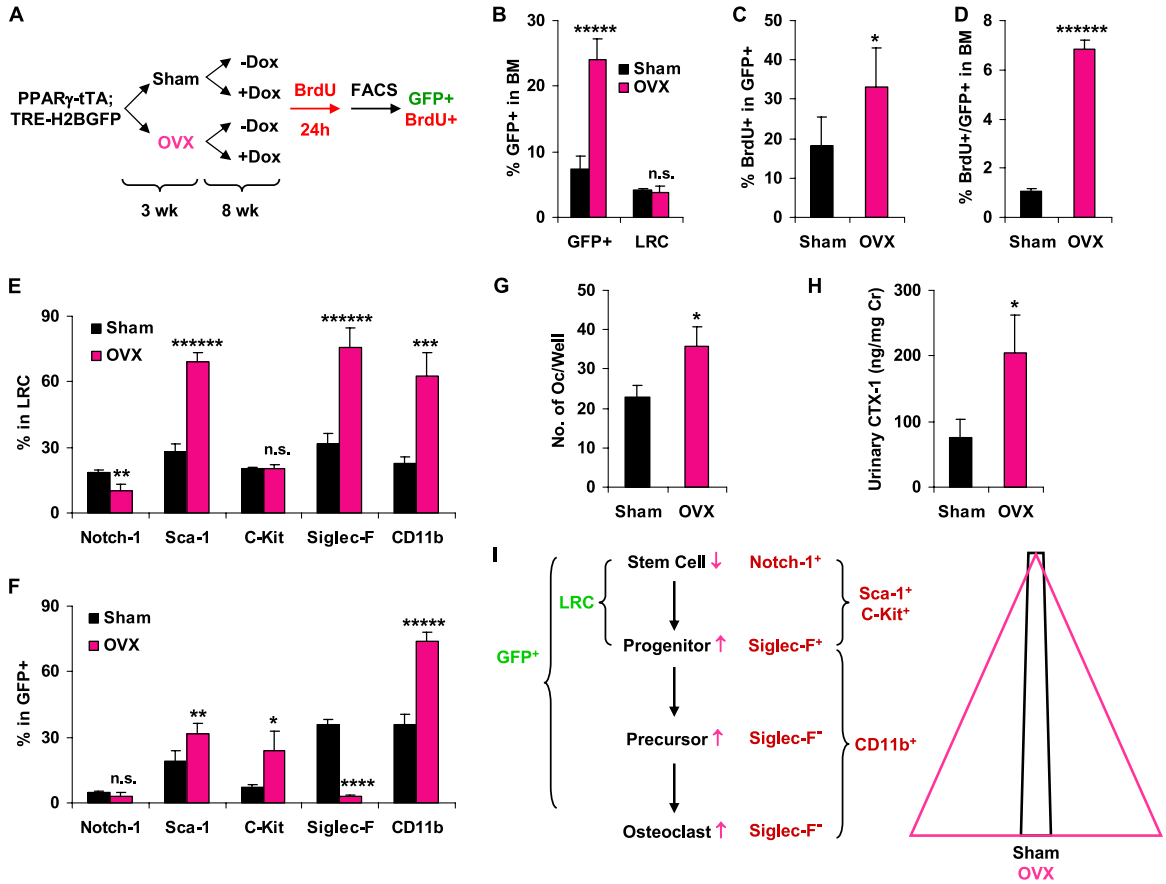

FIG. 5. Ovariectomy triggers osteoclast progenitors to differentiate. (A) Flow chart of the pulse-chase experiment in OVX mice and sham-treated controls (2 months old; female; $n = 4$). (B) Percentages of total GFP$^+$ and LRC populations in bone marrow cells. The error bars indicate SD. (C) Percentage of BrdU$^+$ cells in the total GFP$^+$ bone marrow population. (D) Percentage of GFP$^+$/BrdU$^+$ cells in the entire bone marrow population. (E) Percentages of cells expressing stem/progenitor cell markers (Notch-1, Sca-1, C-Kit, or Siglec-F) and monocyte/macrophage marker (CD11b) in the LRC population. (F) Percentages of cells expressing stem/progenitor cell markers (Notch-1, Sca-1, C-Kit, or Siglec-F) and monocyte/macrophage marker (CD11b) in the total GFP$^+$ population. (G) Osteoclast differentiation assay of GFP$^+$ bone marrow cells from OVX mice and sham-treated controls ($n = 3$). (H) Urinary CTX-1. (I) Model of OVX stimulation of osteoclast precursor proliferation and differentiation. (Left) The pink arrows indicate OVX-induced changes in each cell population. (Right) The pink triangle and the black trapezoid illustrate the relative subpopulation distributions in OVX and sham-treated mice. *, $P < 0.05$; **, $P < 0.01$; ***, $P < 0.005$; *****, $P < 0.0005$; ******, $P < 0.0001$; n.s., nonsignificant ($P > 0.05$).

genitors (LRCs; +Dox) (Fig. 5E) and osteoclast precursors (total GFP$^+$; −Dox) (Fig. 5F). We observed that the percentage of LRCs in total GFP$^+$ cells (LRC/GFP$^+$) was 15% in OVX mice compared to 66% in sham controls (66%), resulting in a 4.2-fold reduction (Fig. 5B). The percentage of stem cells (Notch-1$^+$) was decreased, while the percentage of progenitor cells (Sca1$^+$ or c-Kit$^+$) was increased (Fig. 5E and F). These results suggested that OVX triggered the quiescence-to-proliferation switch of the osteoclast progenitors. Furthermore, Siglec-F is predominantly expressed in immature myelomonocytic precursors, and its expression is reduced upon macrophage/osteoclast differentiation (3). We found that the percentage of Siglec-F$^+$ cells was increased in the LRCs but decreased in the GFP$^+$ population (Fig. 5E and F), suggesting that OVX triggered not only the proliferation of the LRC progenitors, but also the differentiation of the GFP$^+$ precursors. This notion was further illustrated by the elevated percentage of monocyte/macrophage lineage-committed cells (CD11b$^+$) (Fig. 5E and F). Moreover, osteoclast differentiation assays showed that when equal numbers of GFP$^+$ cells were seeded, more osteoclasts formed for the OVX mice than for the sham-treated controls (Fig. 5G), indicating that OVX increased both the number of GFP$^+$ cells in the bone marrow and their differentiation potential. Consequently, OVX led to increased resorption (Fig. 5H). Together, these results indicate that OVX activated both the quiescence-to-proliferation switch in osteoclast progenitors and the proliferation-to-differentiation switch in osteoclast precursors (Fig. 5I), revealing previously unrecognized effects of estrogen deficiency on early osteoclast lineage specification.

Pharmacological activation of osteoclast progenitors. The tracking system also allowed us to examine the response of the osteoclast lineage to drugs. As a model, we chose BRL, a PPARγ agonist and a diabetic drug that stimulates osteoclast differentiation and bone resorption (52, 53, 59). In *ex vivo* cultures, BRL attenuated M-CSF-mediated osteoclast precursor proliferation (Fig. 6A) yet exacerbated RANKL induction of osteoclast markers (c-fos and TRAP) (Fig. 6B), suggesting

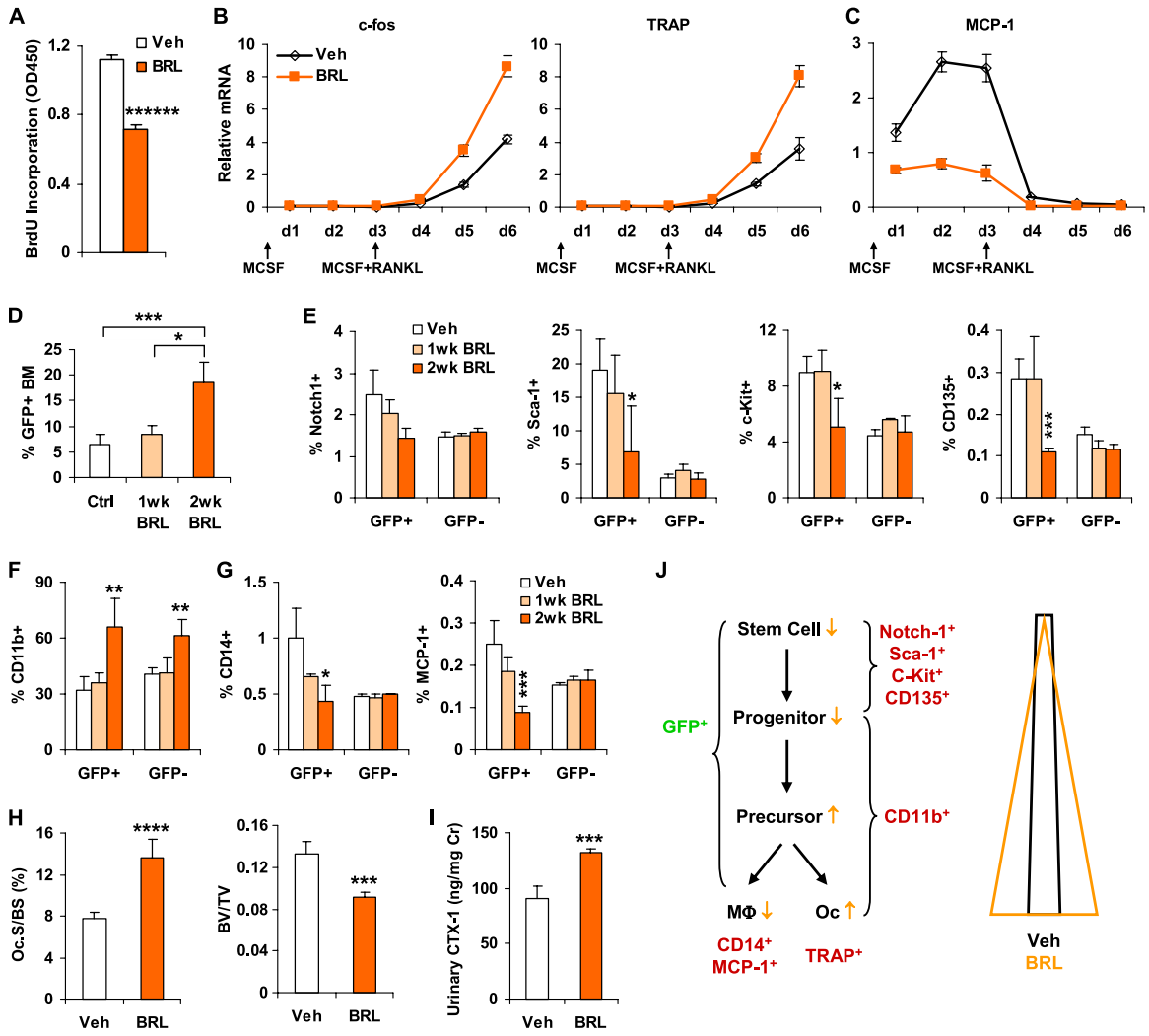

FIG. 6. Ligand activation of PPARγ triggers osteoclast progenitors to differentiate. (A) BRL attenuated osteoclast precursor proliferation *ex vivo* ($n = 3$). The error bars indicate SD. (B and C) BRL stimulated RANKL-mediated induction of osteoclast markers (B) but inhibited mature macrophage markers (C) during a 6-day time course of *ex vivo* osteoclast differentiation ($n = 3$). The arrows indicate the addition of M-CSF at day 0 and the addition of M-CSF plus RANKL at day 3. (D to G) FACS analyses of the effects of BRL on osteoclast progenitors/precursors *in vivo*. PPARγ-GFP mice (6 months old; male; $n = 4$) were treated with BRL (10 mg/kg of body weight/day) or vehicle (Veh) for 1 or 2 weeks. (D) Percentages of GFP^+ cells in bone marrow. (E) Percentages of cells expressing stem cell markers in GFP^+ and GFP^- populations. (F) Percentages of cells expressing pan-monocyte/macrophage marker. (G) Percentages of cells expressing mature macrophage markers. (H and I) Effects of BRL on osteoclast number and bone resorption *in vivo*. Mice were treated with BRL (10 mg/kg/day) or vehicle for 8 weeks ($n = 4$). (H) Osteoclast surface and BV/TV ratio. (I) Urinary CTX-1. (J) Model for BRL stimulation of osteoclast differentiation *in vivo*. (Left) The orange arrows indicate BRL-induced changes in each cell population. (Right) The orange triangle and the black trapezoid illustrate the relative subpopulation distributions in BRL- and Veh-treated mice. *, $P < 0.05$; **, $P < 0.01$; ***, $P < 0.005$; ****, $P < 0.001$; ******, $P < 0.0001$.

that PPARγ activation triggers a proliferation-to-differentiation switch toward osteoclasts. Interestingly, both BRL and RANKL suppressed the mature macrophage marker (MCP-1) (Fig. 6C), indicating that BRL promotes an osteoclast fate in part by shifting the progenitors away from a terminal macrophage fate.

To determine the effects of PPARγ activation on the osteoclast lineage *in vivo*, we next administered BRL or vehicle control to the reporter mice. By 2 weeks, BRL increased the GFP^+ population within the marrow by 2.9-fold (Fig. 6D) yet reduced the percentage of stem/progenitor cells ($Notch1^+$, $Sca\text{-}1^+$, $c\text{-}Kit^+$, or $CD135^+$) in the GFP^+ population (Fig. 6E). We did not observe changes in these markers in the GFP^- ($PPAR\gamma^-$) population, indicating that the BRL effects were PPARγ dependent (Fig. 6E). Consistently, BRL increased the macrophage lineage-committed cells ($CD11b^+$) (Fig. 6F) (45). Intriguingly, BRL significantly diminished the percentage of mature macrophages in the GFP^+ population, as both CD14 (a lipopolysaccharide [LPS] receptor) (21) and MCP-1 (58) were downregulated (Fig. 6G). In contrast, BRL increased the osteoclast surface (Fig. 6H) and the bone resorption marker CTX-1 (Fig. 6I), leading to a decreased bone volume/tissue volume (BV/TV) ratio (Fig. 6H) but unaltered bone mineral density (BMD) (not shown). These *in vivo* data were consistent with the *ex vivo* results (Fig. 6B and C), indicating that ligand activation of PPARγ triggered the osteoclast progenitors to

undergo differentiation, but toward osteoclasts and away from mature macrophages (Fig. 6J). Thus, PPARγ$^+$ cells are osteoclast progenitors, yet PPARγ is also a molecular switch that translates an increased local concentration of PPARγ agonists into enhanced osteoclast differentiation. Importantly, both OVX and BRL, representing pathological and pharmacological resorption-enhancing stimuli, triggered the PPARγ$^+$ cells to proliferate and differentiate, further supporting the notion that osteoclast progenitors reside in the PPARγ$^+$ bone marrow population *in vivo*.

PPARγ promotes osteoclast progenitors by activating GATA2 transcription. The GATA family of zinc finger transcription factors is an important regulator of hematopoiesis. GATA2 is required to generate osteoclast progenitors (50, 54), while GATA1 is dispensable for osteoclastogenesis but essential for erythropoiesis and megakaryocyte maturation (20, 37, 43). Therefore, the GATA2/GATA1 ratio in hematopoietic progenitors controls lineage divergence between osteoclasts and erythrocytes/megakaryocytes. In our microarray analysis, we found that this key GATA2/GATA1 ratio was 12.9-fold higher in the PPARγ$^+$ (GFP$^+$) cells than in the PPARγ$^-$ (GFP$^-$) cells (Fig. 7A), owing to elevated GATA2 expression and diminished GATA1 expression (Fig. 7B). Since PPARγ is also critical for osteoclastogenesis (52), it may promote osteoclast progenitor commitment by activating GATA2 transcription.

To test this hypothesis, we examined the GATA2 promoter and identified three highly conserved PPAR response elements (PPREs) (Fig. 7C). To determine whether PPARγ directly binds to the mouse GATA2 promoter and induces its transcription, we performed a ChIP assay with antibodies for PPARγ or acetylated histone H3, a chromatin marker for activated transcription. In GFP$^+$ cells, but not GFP$^-$ control cells, PPARγ bound to all three PPREs in the mGATA2 promoter, accompanied by elevated levels of acetylated histone H3 (Fig. 7D); in contrast, PPARγ did not bind to the GATA1 promoter (not shown), suggesting that PPARγ inhibits GATA1 expression via an indirect mechanism. PU.1 binding was also detected in these GATA2 regions, suggesting that PPARγ colocalization with PU.1 in the GFP$^+$ cells specified GATA2 expression and osteoclast progenitors (Fig. 7D). We next assessed the functional requirement for GATA2 by both gain- and loss-of-function analyses. Ectopic GATA2 expression in PPARγ$^-$ cells to a level comparable to that in PPARγ$^+$ cells partially rescued the osteoclast differentiation blockade (Fig. 7E). Conversely, GATA2 knockdown severely diminished both RANKL-mediated and BRL-stimulated osteoclast differentiation in the PPARγ$^+$ cells (Fig. 7F). Together, these results indicate that PPARγ promotes osteoclast progenitor commitment, at least in part, by directly binding to the GATA2 promoter and activating its transcription (Fig. 7G).

DISCUSSION

The cellular identity and precise nature of osteoclast progenitors are longstanding and important biological questions. Based on our cellular, molecular, genetic, pathological, and pharmacological evidence, *in vivo* and *ex vivo*, we conclude that the osteoclast lineage resides in the PPARγ-expressing hematopoietic bone marrow cell population, and we have identified the quiescent PPARγ$^+$ bone marrow cells as the osteoclast progenitors. Importantly, we have established PPARγ-tTA TRE-H2BGFP reporter mice as an unprecedented tool to visualize, isolate, quantify, and trace the lineage of osteoclast progenitors. As a complement, we have also established PPARγ-tTA TRE-Cre mice as a genetic tool to interrogate the function and regulation of osteoclast progenitors *in vivo* by inducing flox-mediated gene deletion or activation. Using these tools, we have uncovered previously unrecognized effects of ovariectomy and rosiglitazone, two resorption-enhancing stimuli, on the early osteoclast lineage. Mechanistically, we have identified GATA2 as a novel yet critical PPARγ target gene in osteoclast progenitors. Therefore, both conceptually and technically, this study opens an exciting new path to the fundamental understanding of both osteoclast lineage specification and PPARγ function.

In the PPARγ-tTA TRE-H2BGFP reporter mice, GFP$^+$ cells also label adipocyte progenitors and mature adipocytes (46). Intriguingly, several reports show that mammalian cells of the adipocyte lineage and the macrophage lineage share numerous functional and antigenic properties. Gene expression profiling revealed that preadipocytes share a surprisingly closer signature with macrophages than with adipocytes, and preadipocytes can be effectively converted to macrophages in a macrophage environment (10). This appears to be an evolutionarily conserved phenomenon, because in invertebrates, such as *Drosophila*, hemocytes (blood cells) and fat bodies also share the expression of fate-determining genes (14). Our findings that PPARγ$^+$ cells label both adipocyte progenitors and macrophage/osteoclast progenitors provided mechanistic evidence for convergence and/or plasticity in the adipocyte and macrophage lineage specification. Together with the dual roles of PPARγ ligand in stimulating both adipogenesis and osteoclastogenesis, our findings illuminate a potential molecular basis for the close correlation between insulin-sensitizing effects and bone loss effects, as well as the emerging connections between fat and bone.

Stem/progenitor cells are defined as multipotent; hence, in order to target osteoclast progenitors experimentally, it is impossible to completely rule out other differentiation outcomes, and specificity is only relative. For example, Tie2 labels not only osteoclast progenitors, but also all other hematopoietic progenitors, as well as endothelial cells (13, 52), whereas PPARγ labels osteoclast and adipocyte progenitors but not other hematopoietic lineages (Fig. 1 and 2). The advantages of the PPARγ-tTA-based mouse models include the following: (i) they distinguish macrophages/osteoclasts from other hematopoietic lineages; (ii) they target the entire osteoclast lineage, including osteoclast progenitors and mature osteoclasts; and (iii) they permit temporal control of inducible cell labeling and genetic manipulations in the osteoclast lineage. Our results show that osteoclast progenitors are 140-fold enriched in the PPARγ$^+$ bone marrow cell population, and thus, only $<1\%$ of osteoclast progenitors may be derived from PPARγ^{low} or PPARγ$^-$ cells. Moreover, previous studies have documented that Notch activation in lymphoid progenitors causes T-cell lymphoblastic leukemia in humans and mice (16, 36). In our study, PTNICD mice did not develop lymphoma, which further supports the notion that PPARγ specifically directs hematopoiesis toward the monocyte/macrophage lineage and that the

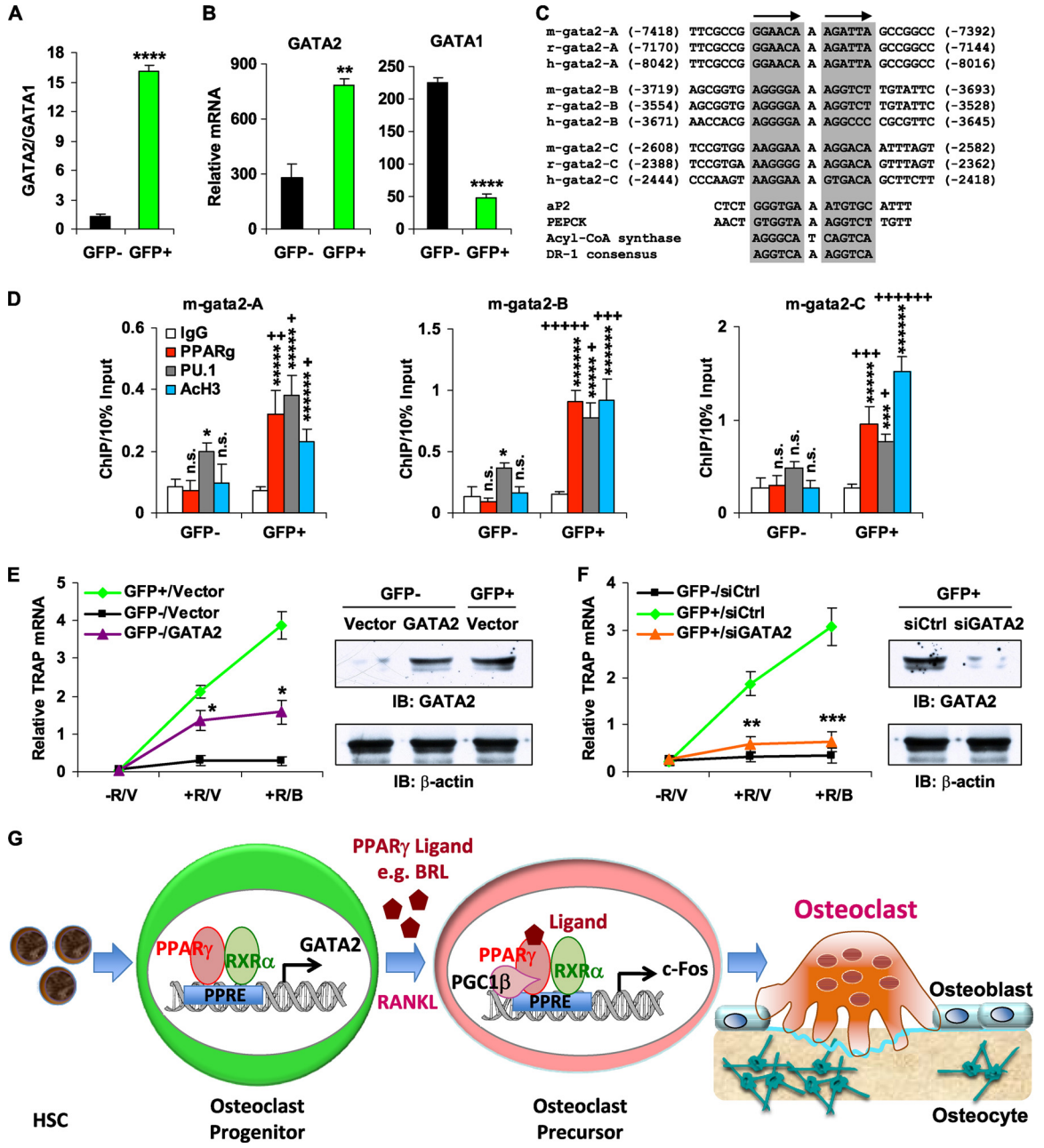

FIG. 7. PPARγ promotes osteoclast progenitors by activating GATA2 transcription. (A) GATA2/GATA1 mRNA ratio in GFP$^+$ and GFP$^-$ bone marrow populations ($n = 2$). The error bars indicate SD. (B) GATA2 and GATA1 mRNA expression ($n = 2$). (C) Alignment of mouse (m), rat (r), and human (h) GATA2 promoter PPRE regions, together with known PPREs for ap2, PEPCK, ACS, and DR-1 consensus. (D) ChIP analysis of PPARγ or PU.1 binding and histone H3 acetylation in the mGATA2 promoter PPRE regions in GFP$^-$ and GFP$^+$ bone marrow cells. For P values, the asterisks (or n.s.) compare each antibody with IgG control in the same cell population; the pluses compare the same antibody in GFP$^+$ cells with GFP$^-$ cells ($n = 3$). (E) Osteoclast differentiation blockade in PPARγ$^-$ cells was partially rescued by ectopic GATA2 expression. Hematopoietic bone marrow cells were transfected with GATA2-expressing plasmid or vector control. Osteoclast differentiation was quantified by TRAP expression (left), and GATA2 protein was quantified by Western blotting (IB) (right). The P values compare GATA2-transfected GFP$^-$ cells with vector-transfected GFP$^-$ cells; GFP$^+$ cells served as a positive control. (F) RANKL-induced and BRL-stimulated osteoclast differentiation in PPARγ$^+$ cells was severely diminished by GATA2 knockdown. Hematopoietic bone marrow cells were transfected with GATA2 siRNA (siGATA2) or control siRNA (siCtrl). Osteoclast differentiation was quantified by TRAP expression (left), and GATA2 protein was quantified by Western blotting (right). The P values compare siGATA2-transfected GFP$^+$ cells with siCtrl-transfected GFP$^+$ cells; GFP$^-$ cells served as a negative control. (G) Model for PPARγ regulation of osteoclastogenesis. PPARγ expression promotes osteoclast progenitor specification by activating GATA2 transcription. Upon PPARγ agonist availability, the ligand-activated PPARγ/RXRα receptor complex recruits coactivator PGC1β and induces c-fos transcription, thereby stimulating RANKL-mediated osteoclast differentiation. HSC, hematopoietic stem cells. * or +, $P < 0.05$; ** or ++, $P < 0.01$; *** or +++, $P < 0.005$; ****, $P < 0.001$; ***** or +++++, $P < 0.0005$; ****** or ++++++, $P < 0.0001$; n.s., nonsignificant ($P > 0.05$).

PPARγ-expressing bone marrow population does not contain lymphoid progenitors. Since PPARγ also labels adipocyte progenitors (46), it is possible that Notch constitutive activation in PTNICD mice may also affect other PPARγ$^+$ cells, such as adipocytes, in addition to osteoclast progenitors.

Several drivers targeting macrophage precursors or mature osteoclasts have been elegantly described; nonetheless, because they do not target osteoclast progenitors, they are not suitable for *in vivo* study of early osteoclast lineage specification. For example, CD11b or lysozyme drivers are useful to target macrophage precursors because they are upregulated only upon macrophage differentiation (12, 19, 25). In addition, Ctsk or TRAP drivers are useful to target preosteoclasts and mature osteoclasts because they are upregulated only upon osteoclast differentiation (11, 34). Therefore, the PPARγ-tTA-based models represent a novel osteoclast progenitor-targeting strategy that is complementary to other existing models for the comprehensive investigation of osteoclast lineage specification and differentiation.

Indeed, the PTNICD and PTDTA genetic models provide compelling *in vivo* evidence that the osteoclast lineage resides in the PPARγ$^+$ bone marrow population under physiological conditions; in particular, the PTNICD model supports the notion that PPARγ$^+$ cells represent osteoclast progenitors. In the PTDTA model, the DTA was an "attenuated" version of diphtheria toxin, thus explaining the relatively mild bone phenotype, which was supported by the survival of the PTDTA mice in contrast to the embryonic lethality in the global PPARγ knockout (KO) mice (7, 28, 40). Furthermore, both OVX and BRL, representing pathological and pharmacological resorption-enhancing stimuli, triggered the PPARγ$^+$ cells to proliferate and differentiate, further supporting the notion that osteoclast progenitors reside in the PPARγ$^+$ bone marrow population *in vivo*. The rapid increase (1 to 2 weeks) in the percentage of GFP$^+$ bone marrow cells in response to BRL treatment *in vivo* indicates that this effect was not likely secondary to any BRL alteration of adipocytes followed by changes in hematopoiesis, which takes at least 4 weeks (1).

The Ets family transcription factor PU.1 is essential for the development of both myeloid and B-lymphoid cells (42). This suggests that additional transcription factors are required to function in combination with PU.1 and confer lineage specificity (22). Since osteoclasts are of myeloid lineage, PU.1 is also essential for the generation of osteoclast progenitors. Indeed, PU.1 deletion in mice precludes osteoclast development, leading to arrested bone resorption and osteopetrosis (47). A recent study revealed that, in macrophages, PPARγ colocalizes with PU.1 in areas of open chromatin and histone acetylation near a distinct set of hematopoietic genes (31). Our results suggest that in the PPARγ$^+$ cells, PPARγ cooperates with PU.1 to activate the transcription of a subset of genes, including GATA2, thereby directing macrophage/osteoclast lineage commitment. In contrast, in the PPARγ$^-$ cells, the absence of PPARγ prevents GATA2 transcription and alters the subset of genes regulated by PU.1, thereby directing B-lymphoid lineage commitment. Therefore, our identification of PPARγ$^+$ bone marrow cells as osteoclast progenitors provides *in vivo* evidence for the notion that the collaborative interaction between PPARγ and PU.1 on a subset of promoters is essential to activate the transcriptional program required for macrophage/osteoclast lineage commitment. Furthermore, our results suggest that the expression of PPARγ, rather than the ligand activation of PPARγ, promotes osteoclast progenitor specification by enhancing GATA2 expression, which is downregulated during the quiescence-to-proliferation switch and thus is absent in osteoclast precursors (53a) (Fig. 7G). Together, our current and previous studies reveal that PPARγ plays dual roles in osteoclastogenesis that involve multiple mechanisms and target genes (Fig. 7G): PPARγ expression promotes osteoclast progenitors by inducing GATA2, and PPARγ ligand activation stimulates osteoclast differentiation by inducing c-fos.

ACKNOWLEDGMENTS

We thank J. Zerwekh for assistance with bone histomorphometry, L. Smith for assistance with μCT, and D. Mangelsdorf and S. Kliewer for helpful discussion.

This work was supported by the University of Texas Southwestern Medical Center Endowed Scholar Startup Fund (Y.W.), a BD Biosciences Research Grant Award (Y.W.), CPRIT (RP100841 [Y.W.]), the March of Dimes (5-FY10-1 [Y.W.]), The Welch Foundation (I-1751 [Y.W.]), NIH (R01 DK089113 [Y.W.] and R01 DK066556, R01 DK064261, and R01 DK088220 [J.M.G.]), and a postdoctoral fellowship (W.T.) and a predoctoral fellowship (D.Z.) from the American Heart Association South Central Affiliate. Y.W. is a Virginia Murchison Linthicum Scholar in Medical Research.

J.M.G. is a founder of Reata Pharmaceuticals. We declare that we have no financial conflict of interest.

REFERENCES

1. **Ali, A. A., et al.** 2005. Rosiglitazone causes bone loss in mice by suppressing osteoblast differentiation and bone formation. Endocrinology **146:**1226–1235.
2. **Anderson, D. M., et al.** 1990. Molecular cloning of mast cell growth factor, a hematopoietin that is active in both membrane bound and soluble forms. Cell **63:**235–243.
3. **Angata, T., R. Hingorani, N. M. Varki, and A. Varki.** 2001. Cloning and characterization of a novel mouse Siglec, mSiglec-F: differential evolution of the mouse and human (CD33) Siglec-3-related gene clusters. J. Biol. Chem. **276:**45128–45136.
4. **Arai, F., et al.** 1999. Commitment and differentiation of osteoclast precursor cells by the sequential expression of c-Fms and receptor activator of nuclear factor kappaB (RANK) receptors. J. Exp. Med. **190:**1741–1754.
5. **Ash, P., J. F. Loutit, and K. M. Townsend.** 1980. Osteoclasts derived from haematopoietic stem cells. Nature **283:**669–670.
6. **Bai, S., et al.** 2008. NOTCH1 regulates osteoclastogenesis directly in osteoclast precursors and indirectly via osteoblast lineage cells. J. Biol. Chem. **283:**6509–6518.
7. **Barak, Y., et al.** 1999. PPAR gamma is required for placental, cardiac, and adipose tissue development. Mol. Cell **4:**585–595.
8. **Boyle, W. J., W. S. Simonet, and D. L. Lacey.** 2003. Osteoclast differentiation and activation. Nature **423:**337–342.
9. **Chamberlain, G., J. Fox, B. Ashton, and J. Middleton.** 2007. Concise review: mesenchymal stem cells: their phenotype, differentiation capacity, immunological features, and potential for homing. Stem Cells **25:**2739–2749.
10. **Charriere, G., et al.** 2003. Preadipocyte conversion to macrophage. Evidence of plasticity. J. Biol. Chem. **278:**9850–9855.
11. **Chiu, W. S., et al.** 2004. Transgenic mice that express Cre recombinase in osteoclasts. Genesis **39:**178–185.
12. **Clausen, B. E., C. Burkhardt, W. Reith, R. Renkawitz, and I. Forster.** 1999. Conditional gene targeting in macrophages and granulocytes using LysMcre mice. Transgenic Res. **8:**265–277.
13. **Constien, R., et al.** 2001. Characterization of a novel EGFP reporter mouse to monitor Cre recombination as demonstrated by a Tie2 Cre mouse line. Genesis **30:**36–44.
14. **de Velasco, B., L. Mandal, M. Mkrtchyan, and V. Hartenstein.** 2006. Subdivision and developmental fate of the head mesoderm in Drosophila melanogaster. Dev. Genes Evol. **216:**39–51.
15. **Dougall, W. C., et al.** 1999. RANK is essential for osteoclast and lymph node development. Genes Dev. **13:**2412–2424.
16. **Ellisen, L. W., et al.** 1991. TAN-1, the human homolog of the Drosophila notch gene, is broken by chromosomal translocations in T lymphoblastic neoplasms. Cell **66:**649–661.
17. **Engin, F., et al.** 2008. Dimorphic effects of Notch signaling in bone homeostasis. Nat. Med. **14:**299–305.

18. **Evans, R. M., G. D. Barish, and Y. X. Wang.** 2004. PPARs and the complex journey to obesity. Nat. Med. **10:**355–361.
19. **Ferron, M., and J. Vacher.** 2005. Targeted expression of Cre recombinase in macrophages and osteoclasts in transgenic mice. Genesis **41:**138–145.
20. **Fujiwara, Y., C. P. Browne, K. Cunniff, S. C. Goff, and S. H. Orkin.** 1996. Arrested development of embryonic red cell precursors in mouse embryos lacking transcription factor GATA-1. Proc. Natl. Acad. Sci. U. S. A. **93:** 12355–12358.
21. **Haziot, A., et al.** 1996. Resistance to endotoxin shock and reduced dissemination of gram-negative bacteria in CD14-deficient mice. Immunity **4:**407–414.
22. **Heinz, S., et al.** 2010. Simple combinations of lineage-determining transcription factors prime cis-regulatory elements required for macrophage and B cell identities. Mol. Cell **38:**576–589.
23. **Hermiston, M. L., J. Zikherman, and J. W. Zhu.** 2009. CD45, CD148, and Lyp/Pep: critical phosphatases regulating Src family kinase signaling networks in immune cells. Immunol. Rev. **228:**288–311.
24. **Huang, E., et al.** 1990. The hematopoietic growth factor KL is encoded by the Sl locus and is the ligand of the c-kit receptor, the gene product of the W locus. Cell **63:**225–233.
25. **Jacquin, C., D. E. Gran, S. K. Lee, J. A. Lorenzo, and H. L. Aguila.** 2006. Identification of multiple osteoclast precursor populations in murine bone marrow. J. Bone Miner. Res. **21:**67–77.
26. **Kanda, T., K. F. Sullivan, and G. M. Wahl.** 1998. Histone-GFP fusion protein enables sensitive analysis of chromosome dynamics in living mammalian cells. Curr. Biol. **8:**377–385.
27. **Krum, S. A., et al.** 2008. Estrogen protects bone by inducing Fas ligand in osteoblasts to regulate osteoclast survival. EMBO J. **27:**535–545.
28. **Kubota, N., et al.** 1999. PPAR gamma mediates high-fat diet-induced adipocyte hypertrophy and insulin resistance. Mol. Cell **4:**597–609.
29. **Lacey, D. L., et al.** 1998. Osteoprotegerin ligand is a cytokine that regulates osteoclast differentiation and activation. Cell **93:**165–176.
30. **Lee, P., et al.** 1998. Conditional lineage ablation to model human diseases. Proc. Natl. Acad. Sci. U. S. A. **95:**11371–11376.
31. **Lefterova, M. I., et al.** 2010. Cell-specific determinants of PPAR{gamma} function in adipocytes and macrophages. Mol. Cell. Biol. **30:**2078–2089.
32. **Marshall, M. J., and M. W. Davie.** 1991. An immunocytochemical method for studying the kinetics of osteoclast nuclei on intact mouse parietal bone. Histochem. J. **23:**402–408.
33. **Matthews, W., C. T. Jordan, G. W. Wiegand, D. Pardoll, and I. R. Lemischka.** 1991. A receptor tyrosine kinase specific to hematopoietic stem and progenitor cell-enriched populations. Cell **65:**1143–1152.
34. **Nakamura, T., et al.** 2007. Estrogen prevents bone loss via estrogen receptor alpha and induction of Fas ligand in osteoclasts. Cell **130:**811–823.
35. **Novack, D. V., and S. L. Teitelbaum.** 2008. The osteoclast: friend or foe? Annu. Rev. Pathol. **3:**457–484.
36. **Pear, W. S., et al.** 1996. Exclusive development of T cell neoplasms in mice transplanted with bone marrow expressing activated Notch alleles. J. Exp. Med. **183:**2283–2291.
37. **Pevny, L., et al.** 1991. Erythroid differentiation in chimaeric mice blocked by a targeted mutation in the gene for transcription factor GATA-1. Nature **349:**257–260.
38. **Pittenger, M. F., et al.** 1999. Multilineage potential of adult human mesenchymal stem cells. Science **284:**143–147.
39. **Ricote, M., A. C. Li, T. M. Willson, C. J. Kelly, and C. K. Glass.** 1998. The peroxisome proliferator-activated receptor-gamma is a negative regulator of macrophage activation. Nature **391:**79–82.
40. **Rosen, E. D., et al.** 1999. PPAR gamma is required for the differentiation of adipose tissue in vivo and in vitro. Mol. Cell **4:**611–617.
41. **Scheven, B. A., J. W. Visser, and P. J. Nijweide.** 1986. In vitro osteoclast generation from different bone marrow fractions, including a highly enriched haematopoietic stem cell population. Nature **321:**79–81.
42. **Scott, E. W., M. C. Simon, J. Anastasi, and H. Singh.** 1994. Requirement of transcription factor PU.1 in the development of multiple hematopoietic lineages. Science **265:**1573–1577.
43. **Shivdasani, R. A., Y. Fujiwara, M. A. McDevitt, and S. H. Orkin.** 1997. A lineage-selective knockout establishes the critical role of transcription factor GATA-1 in megakaryocyte growth and platelet development. EMBO J. **16:**3965–3973.
44. **Spangrude, G. J., S. Heimfeld, and I. L. Weissman.** 1988. Purification and characterization of mouse hematopoietic stem cells. Science **241:**58–62.
45. **Springer, T., G. Galfre, D. S. Secher, and C. Milstein.** 1979. Mac-1: a macrophage differentiation antigen identified by monoclonal antibody. Eur. J. Immunol. **9:**301–306.
46. **Tang, W., et al.** 2008. White fat progenitor cells reside in the adipose vasculature. Science **322:**583–586.
47. **Tondravi, M. M., et al.** 1997. Osteopetrosis in mice lacking haematopoietic transcription factor PU. 1. Nature **386:**81–84.
48. **Tontonoz, P., L. Nagy, J. G. Alvarez, V. A. Thomazy, and R. M. Evans.** 1998. PPARgamma promotes monocyte/macrophage differentiation and uptake of oxidized LDL. Cell **93:**241–252.
49. **Tontonoz, P., and B. M. Spiegelman.** 2008. Fat and beyond: the diverse biology of PPARgamma. Annu. Rev. Biochem. **77:**289–312.
50. **Tsai, F. Y., et al.** 1994. An early haematopoietic defect in mice lacking the transcription factor GATA-2. Nature **371:**221–226.
51. **Tumbar, T., et al.** 2004. Defining the epithelial stem cell niche in skin. Science **303:**359–363.
52. **Wan, Y., L. W. Chong, and R. M. Evans.** 2007. PPAR-gamma regulates osteoclastogenesis in mice. Nat. Med. **13:**1496–1503.
53. **Wei, W., et al.** 2010. PGC1beta mediates PPARgamma activation of osteoclastogenesis and rosiglitazone-induced bone loss. Cell Metab. **11:**503–516.

53a. **Wei, W., et al.** 2011. Biphasic and dosage-dependent regulation of osteoclastogenesis by β-catenin. Mol. Cell. Biol. **31:**4706–4719.

54. **Yamane, T., et al.** 2000. Sequential requirements for SCL/tal-1, GATA-2, macrophage colony-stimulating factor, and osteoclast differentiation factor/osteoprotegerin ligand in osteoclast development. Exp. Hematol. **28:**833–840.
55. **Yang, X., et al.** 2004. Notch activation induces apoptosis in neural progenitor cells through a p53-dependent pathway. Dev. Biol. **269:**81–94.
56. **Yasuda, H., et al.** 1998. Osteoclast differentiation factor is a ligand for osteoprotegerin/osteoclastogenesis-inhibitory factor and is identical to TRANCE/RANKL. Proc. Natl. Acad. Sci. U. S. A. **95:**3597–3602.
57. **Yoshida, H., et al.** 1990. The murine mutation osteopetrosis is in the coding region of the macrophage colony stimulating factor gene. Nature **345:**442–444.
58. **Yoshimura, T., et al.** 1989. Human monocyte chemoattractant protein-1 (MCP-1). Full-length cDNA cloning, expression in mitogen-stimulated blood mononuclear leukocytes, and sequence similarity to mouse competence gene JE. FEBS Lett. **244:**487–493.
59. **Zinman, B., et al.** 2010. Effect of rosiglitazone, metformin, and glyburide on bone biomarkers in patients with type 2 diabetes. J. Clin. Endocrinol. Metab. **95:**134–142.
60. **Zsebo, K. M., et al.** 1990. Stem cell factor is encoded at the Sl locus of the mouse and is the ligand for the c-kit tyrosine kinase receptor. Cell **63:**213–224.